

Original Research Article

A structural-based computational model of tendon–bone insertion tissues

Sergey Kuznetsov, Mark Pankow, Kara Peters, Hsiao-Ying Shadow Huang*

North Carolina State University, United States of America



ARTICLE INFO

Keywords:

Functionally graded materials
 Graded microstructure
 Shape optimization
 Biaxial mechanical testing
 Fiber dispersion
 Constitutive model

ABSTRACT

Tendon-to-bone insertion provides a gradual transition from soft tendon to hard bone tissue, functioning to alleviate stress concentrations at the junction of these tissues. Such macroscopic mechanical properties are achieved due to the internal structure in which collagen fibers and mineralization levels are key ingredients. We develop a structural-based model of tendon-to-bone insertion incorporating such details as fiber preferred orientation, fiber directional dispersion, mineralization level, and their inhomogeneous spatial distribution. A python script is developed to alter the tapered tendon–bone transition zone and to provide spatial grading of material properties, which may be rather complex as experiments suggest. A simple linear interpolation between tendon and bone material properties is first used to describe the graded property within the insertion region. Stress distributions are obtained and compared for spatially graded and various piece-wise materials properties. It is observed that spatial grading results in more smooth stress distributions and significantly reduces maximum stresses. The geometry of the tissue model is optimized by minimizing the peak stress to mimic in-vivo tissue remodeling. The in-silico elastic models constructed in this work are verified and modified by comparing to our in-situ biaxial mechanical testing results, thereby serving as translational tools for accurately predicting the material behavior of the tendon-to-bone insertions. This model will be useful for understanding how tendon-to-bone insertion develops during tissue remodeling, as well as for developing orthopedic implants.

1. Introduction

The tendon-to-bone insertion (or “enthesis”) is approximately millimeters-wide region connecting soft and highly transverse isotropic tendon tissue to the stiff and orthotropic bone [1]. The elastic modulus mismatch between tendon and bone is about two orders of magnitude [1,2], making the connection extremely prone to stress concentrations and rupture. Therefore, the insertion site not only transmits contractile forces from muscles to the skeleton, it also balances the elastic moduli of the tendon and bone by dissipating stress away from the junction to avoid local stress peaks at the interface of highly dissimilar materials and to prevent rupture or injury of the tendon and surrounding tissues [3,4]. Inhomogeneity and discontinuities in tissue-level properties, as well as the shape of the natural, uninjured insertion, manifest in a unique, stress-reducing material behavior at the macroscale level. This is achieved by providing a smooth, gradual transition of structural features and composition from soft tendon to hard bone tissue [2,5]. The natural grading between tendon and bone observed in uninjured insertion tissue is not regenerated during tissue healing after rupture, even following surgical interventions, resulting in an inferior connection between these two tissues [1]. Healing of ruptured enthesis with restoration of the natural material inhomogeneity

is an important medical challenge [6]. Therefore, understanding the development, function, and healing of the insertion is important for better designs of prosthetic implants.

At the microscopic level, collagen fibers are key mechanical components in the structure of tendon [7,8], bone, and the insertion between them. On the tendon side of the junction, collagen fibers are dense and aligned along the same direction with very little dispersion in orientation [5,9]. In contrast, collagen fibers are more randomly dispersed in the bone area, resulting in nearly isotropic material properties [1]. Bone and tendon sides are characterized by the predominant concentration of type I collagen. The intermediate region contains fibrocartilage with predominantly type II, III, and X collagen fibers and proteoglycans [2]. A study of composition and structure of porcine digital flexor insertion region via a 2D Fast Fourier Transform was conducted recently by our group [5] and it showed various angles of fiber orientation at the interface of the insertion and bone regions, suggesting that collagen fiber directions are not always normal to the tidemark along the insertion. It also suggested that collagen fiber distribution at the tendon end was highly anisotropic with low dispersion. Randomly distributed fibers were observed at the bone end, and intermediate fiber distribution and dispersion were observed within

* Correspondence to: Mechanical and Aerospace Engineering Department, North Carolina State University, R3158 Engineering Building 3, Campus Box 7910, 911 Oval Drive, Raleigh, NC 27695, United States of America.

E-mail address: hshuang@ncsu.edu (H.-Y.S. Huang).

<https://doi.org/10.1016/j.mbs.2020.108411>

Received 31 October 2019; Received in revised form 28 June 2020; Accepted 28 June 2020

Available online 2 July 2020

0025-5564/© 2020 Elsevier Inc. All rights reserved.

the insertion region. Further, we used Time-of-Flight Secondary Ion Mass Spectrometry (ToF-SIMS) to identify a linear variation of minerals content from bone to tendon section, where the mineral hydroxyapatite is present as tiny crystals along the length of collagen [5]. As shown in Fig. 1, a graded distribution of collagen fibers is also observed by bright field microscopy of stained tissues. Collagen fibers are crimped in the unstressed tissue and become active in tension only. During deformations fibers uncrimp, rotate and become stretched at different times due to the differences in the extended “free” length, i.e. there is a gradual recruitment of the fibers [9–12]. Types of collagen is also varying; Collagen I is rich at the tendons side, collagen II and III are rich in the fibrocartilagenous region, collagen II and X are found in the mineralized fibrocartilagenous region and collagen I is rich again in the bone region [2]. Another important characteristic of the insertion site is the onset and gradual increase in the mineralization level [2], which occurs within intermediate fibrocartilage region. The onset in the mineralization may be observed as a “tidemark”, as shown in Fig. 1.

There is a significant amount of research devoted to modeling or characterizing either tendon [13] or bone tissues [14,15] with their relationship of collagen fibers. It was shown by Y. C. Fung [16,17] that there is a linear relationship between stiffness and stress in biological soft tissues, which suggests an exponential stress–strain relationship for tendons. We will use, therefore, exponential strain energy form in this study. However, other hyperelastic potentials are used as well to model biological tissues [18]. On the other hand, much harder bone tissues experience only small deformations and typical linear stress–strain relations are sufficient [17]. A recent study by Jakus et al. has developed a hyperelastic synthetic bone, which is strong, flexible, and capable of 32%–67% of strain to failure between 4 and 11 MPa elastic modulus [19]. Therefore, even though bone may be considered a linear material, we will consider it as hyperelastic for consistency with tendon and insertion and for possible generalizations, however, the nonlinear part is not expected to contribute under the conditions considered in this paper.

Recently, attention to the tendon-to-bone insertion tissues has started to grow. One of the first attempts to quantitatively describe the organization of the insertion was reported by Thomopoulos et al. [4], where the variation in the collagen fiber orientation was reported. However, the biomechanical characterization was conducted in a general sense, in which a lumped parameter 1D model was used; an exponential law was used for the insertion site to describe the overall mechanical behavior of the insertion tissues [4]. Liu et al. [1] and Thomopoulos et al. [20] considered a distributed finite element models of the tendon-to-bone insertion. However, the insertion was considered as a four-zone structure with piecewise distribution of mean fiber orientation and angular deviation. In their model, the elastic moduli of fibers was approximated linearly with smooth interpolation of the properties between measured values [20], and bone tissue was considered as a rigid body. Liu et al. studied the effect of the angles between bone and insertion tissues on stress concentration and conducted shape optimizations of the insertion to minimize peak stress, again by assuming linear material models for each region (tendon, bone, and insertion) [1]. Spiesz et al. had previously identified the dependence of elastic modulus on the fiber mineralization from mineralized turkey leg tendons [21]. Genin et al. [2,22] and Liu et al. [2,23] considered different models of partially mineralized fibers and related the amount of mineralization to the macroscopic properties of the tissue through averaging across fiber orientations, thus obtaining the dependence of elastic modulus on the mineralization level. Again, this was done using a linear approximation. These models provided important insight into qualitative phenomena occurring at the tendon–bone insertion tissues, but they were limited to linear approximations and could not reflect well the actual behaviors at the insertion site — which is capable of large and highly inhomogeneous deformations.

With the nonlinear nature of the insertion site, interplay between material nonlinearity and structural adjustments during deformations

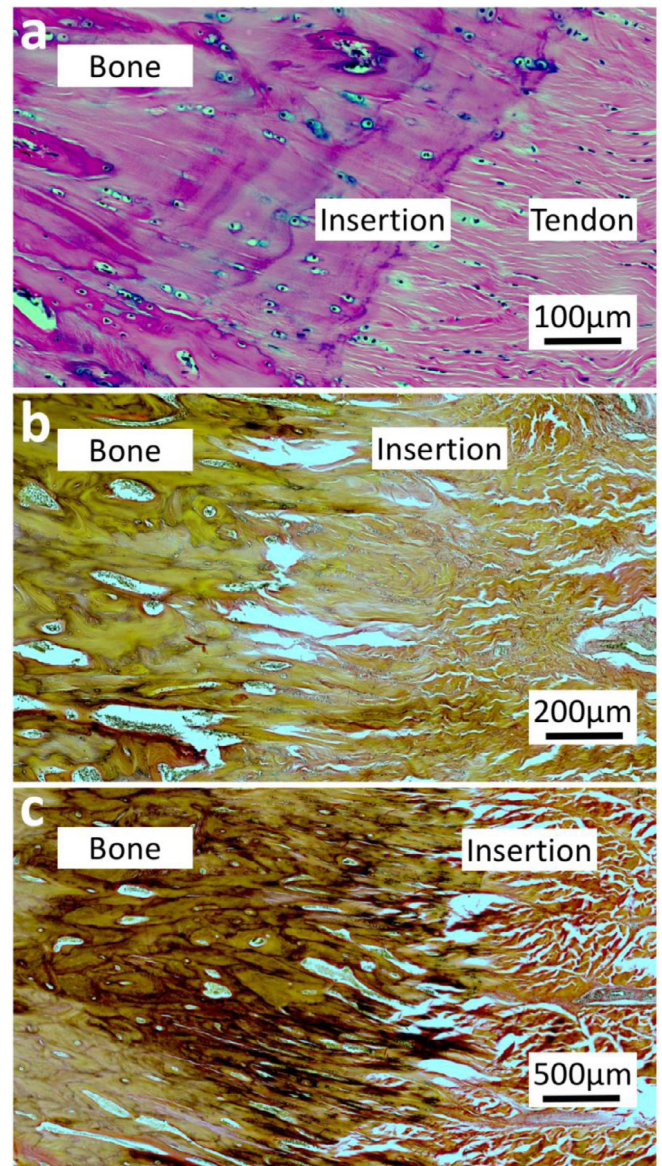


Fig. 1. Brightfield images of porcine (mixed breed sows, from 8-month to 1-year old) digital flexor insertion region at 200 \times magnification (water immersion) obtained using a Zeiss Axioimager (Zeiss Inc., Germany) microscope for sections using (a) Haemotoxylin and Eosin staining and (b) (c) Verhoeff–Van Gieson staining.

should be studied. Therefore, we propose a nonlinear anisotropic hyperelastic model, taking into account inhomogeneous and grading distributions of the material and structural properties of the insertion. We believe that this model will provide deeper insight into the phenomena taking place in the tendon-to-bone insertion.

2. Method

2.1. Constitutive model

The commercial software Dassault Systems (ABAQUS, 2018) (Johnston, Rhode Island) was used for finite element analyses. Based on experimental observations in tendon–bone insertion tissues [5], a linear variation of mineralization level was confirmed by our previous time-of-flight secondary ion mass spectrometry analyses. We then adopted the Gasser–Ogden–Holzapfel (GOH) hyperelastic model [24] to describe varying parameters to capture spatial gradations of mineralization and directional collagen fiber dispersions in tendon–bone

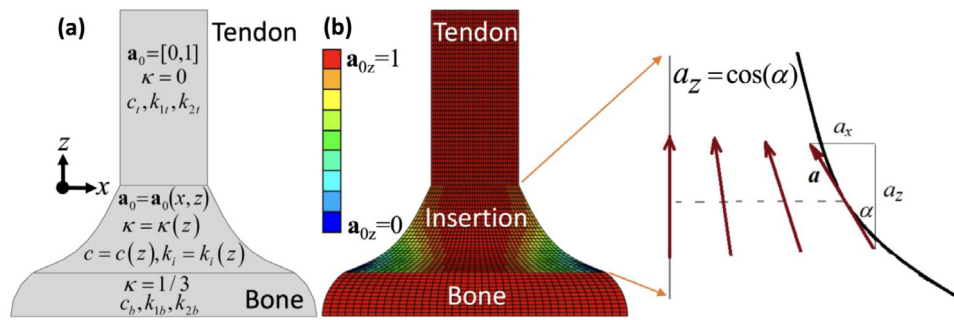


Fig. 2. (a) Simplified geometry of a rotator-cuff model where graded material and structural properties were developed. c : the material parameter to characterize non-collagenous matrix stiffness; k_1 and k_2 : material parameters to describe fiber mechanical responses; κ : a parameter to describe fiber dispersion; \mathbf{a}_0 : preferred fiber orientation. (b) Spatial distribution of preferred fiber orientation, \mathbf{a}_{0z} .

insertion tissues. In addition, a python script was developed to introduce structural grading of preferred fiber orientation, as were observed in histological images (Fig. 1), via a 2D Fast Fourier Transform which was previously published by our group [5]. Initially the GOH model was developed for arterial layers, which are orthotropic materials with two families of fibers [24]. The anisotropic term consisted of two transverse-isotropic contributions, one for each family of fibers. The tendon-to-bone insertion was locally transverse isotropic with only one family of fibers [1,25]. Therefore, only one term of the form was required in the study.

The GOH model was based on the invariant representation of the Helmholtz free energy [26], which was explicitly additively decoupled from the isotropic non-collagenous ground substance contribution Ψ_g and the anisotropic hyperelastic potential term for collagen fibers, Ψ_f . Specifically, the Neo-Hookean model was used to describe the non-collagenous matrix:

$$\Psi_g(I_1) = c(I_1 - 3), \quad (1)$$

where $I_1 = \text{trC}$ was the first invariant of the modified right Cauchy-Green tensor \mathbf{C} [24], and c was the material parameter characterizing non-collagenous matrix stiffness. We noted recently that the Gent model for rubber networks [27] was used for the non-collagenous matrix due to its generality and capacity for reproducing the Neo-Hookean model.

The anisotropic term from the GOH constitutive model featured structural parameters, including fibers in the preferred orientation \mathbf{a}_0 and fibers with directional dispersion $0 \leq \kappa \leq 1/3$ [24,28–30] (Eq. (2)). The continuous spectrum of κ could be used to describe highly aligned fibers with no dispersion ($\kappa = 0$) as observed in tendon tissues, randomly oriented fibers with no preferred orientation (i.e., isotropy when $\kappa = 1/3$) as observed in bone tissues, and all intermediate fiber dispersions occurring in the insertion region (Fig. 1).

$$\Psi_{aniso}(I_1, I_4) = \frac{k_1}{2k_2} \left[\exp \left\{ k_2 \left[\kappa I_1 + (1 - 3\kappa) I_4 - 1 \right]^2 \right\} - 1 \right], \quad (2)$$

where

$$I_4 = \mathbf{a}_0 \otimes \mathbf{a}_0 : \mathbf{C} \quad (3)$$

was a tensor invariant, which characterized stresses in the direction of \mathbf{a}_0 .

In addition, material parameters k_1 and k_2 were used to describe fiber mechanical responses: $k_1 > 0$ was a stress-like material parameter and $k_2 > 0$ was a dimensionless parameter. An appropriate choice of k_1 and k_2 enabled the histologically-based assumption that the collagen fibers do not influence the mechanical response in the low strain domain [28]. The anisotropic term from the GOH constitutive model [24,28–30] provided exponential behavior in accordance with Fung's observation for soft tissues [17].

2.2. Graded material property and collagen fiber microstructure

The GOH model described above contained parameters that include local materials and structural properties. However, it was not capable of capturing responses in distributed inhomogeneous structures. At the same time, Fig. 1 showed that the microstructure within the insertion tissues was continuously graded and that this grading was essential to their mechanical properties. To reflect this important characteristic of the insertion site, one has to introduce spatial gradations along the preferred fiber direction, fiber dispersions, and mechanical properties of collagen fibers and non-collagenous matrix. Therefore, we explicitly introduced a spatial gradation of the aforementioned material properties as follows: $c = c(\mathbf{x})$ in Eq. (1), $k_1 = k_1(\mathbf{x})$, $k_2 = k_2(\mathbf{x})$ in Eq. (2), and structural parameters and $\kappa = \kappa(\mathbf{x})$ in Eq. (2) and $\mathbf{a}_0 = \mathbf{a}_0(\mathbf{x})$ in Eq. (3), where \mathbf{x} was a position vector with coordinates (x, y, z) in 3D space in the reference configuration.

To particularize these dependencies (i.e., fiber dispersion and fiber orientation), we considered a 2D geometry of the porcine rotator-cuff joint adopted from Liu et al. [1] because similar grading behaviors of fiber dispersion and fiber orientation were observed in both rotator-cuff joint and digital flexor insertion [5]. The dimensions of the model were as follows: width of the bone end was 7 cm, width in the tendon end was 2 cm, and height of the model was 7 cm (Fig. 2a). Three domains were identified: the tendon domain denoted as “t” with constant material and structural properties $c_t, k_{1t}, k_{2t}, \kappa_t$; the bone domain denoted as “b” with constant material and structural properties $c_b, k_{1b}, k_{2b}, \kappa_b$; the insertion domain with material and structural properties dependent on the position vector \mathbf{x} . Thus $c = c(x, z)$, $k_1 = k_1(x, z)$, and $k_2 = k_2(x, z)$, where (x, z) were coordinates of a point in 2D space.

Since the exact dependence of material properties at each \mathbf{x} were still unknown, we assumed here the simplest possible case, namely that material properties within the insertion region varied linearly with the longitudinal direction (i.e., z -axis) and were independent of the transverse direction (i.e., x -axis). It was noted, however, that the material property distribution of insertion tissue may be neither linear nor monotonic [1,2,4] since stiffening of collagen fibers due to mineralization was not proportional to the mineralization level and became significant only after a certain percolation threshold — the formation of a mechanical continuous mineral network [2].

It also required that these material properties were continuous at the tendon-insertion and insertion-bone interfaces:

$$c(z) = c_t + d(c_b - c_t) \quad (4)$$

$$k_i(z) = k_{it} + d(k_{ib} - k_{it}), \quad (5)$$

where $i = 1, 2$ and the position parameter d is defined as follows:

$$d = \frac{z_{tendon-insertion} - z}{z_{tendon-insertion} - z_{insertion-bone}}. \quad (6)$$

We also assumed a linear dependence of the structural properties. That is, fiber dispersions only changed along the z -axis:

$$\kappa(z) = d\kappa_{bone} \quad (7)$$

Fig. 2a showed schematically the distribution of $c = c(z)$, $k_1 = k_1(z)$, $k_2 = k_2(z)$, and $\kappa = \kappa(z)$. The preferred collagen fiber orientation was assumed to depend linearly on both the x and z directions. To describe this dependence, we introduced an α -angle between the longitudinal direction and the preferred fiber orientation at any point $\mathbf{x} = \mathbf{x}(x, z)$. This angle was assumed to depend linearly on x with the maximum at the boundary ($x_{boundary}$) and the minimum along the axis of symmetry (x_{axis}) of the model:

$$\alpha(x, z) = \alpha_0(z) \frac{x - x_{axis}}{x_{boundary} - x_{axis}} \quad (8)$$

where α_0 is the angle at the boundary. To simplify the model and to reduce the calculation time, and based on histological images in Fig. 1, preferred fiber orientations may be taken tangential to the boundary and then interpolated toward the axis of symmetry of the model (Fig. 2b). The resulting initial fiber distribution \mathbf{a}_{0z} is shown in Fig. 2b.

In principle, material grading can be introduced into ABAQUS manually. As a result, an in-house python script was developed which utilized its generality and ability to reproduce graded structural and material properties which were incorporated into the GOH constitutive law. Once the tendon–bone insertion geometry was created and meshed, the in-house python script read the ABAQUS input file and identified coordinates for elements (x_e, z_e) (plane stress elements CPS6(S)) belonging to the insertion region. This was followed by the determination of the slope of the boundary at its height z_e and the calculation of fiber preferred orientations $\alpha_0(z_e)$ (Eq. (8)). Next, graded distribution of material and structural properties was created based on the coordinates of each element. Finally, the GOH constitutive law was updated for each element within the insertion region. Of note, with grading introduced in such a way, material properties and structural parameters were constant within each element in the model. That is, the same parameters were used at each integration point in each element.

3. Results

3.1. Material parameters identification

Many studies have reported mechanical properties of connective tissues which were measured primarily through uniaxial tensile tests [31–37]. Such tests were not sufficient to characterize nonlinear and highly anisotropic tissues, as observed *in-vivo* when tissues were under physiological states. Therefore, multiaxial tests such as biaxial stretching tests [38–46] were needed to better approximate states of complex physiologic loads and also to avoid non-physiologic traction-free boundary conditions of uniaxial tension [47,48]. The biaxial mechanical data obtained (i.e. stresses and strains) could be used to formulate constitutive relations.

Here we described the results of experimental stress–strain measurements and the procedure to determine insertion parameters based on the assumptions of linear distributions of structural and material parameters. The porcine digital flexor insertion region was dissected from the joint and was subjected to equi-biaxial displacement-control mechanical testing. We followed mechanical testing procedures described in our previous studies for insertion tissues [49] (Fig. 3a), valvular tissues [41], and dermal skin tissues [42]. Based on the sample dimensions and output data, corresponding nominal stress (i.e., First Piola–Kirchhoff stress) and true strain values were calculated and stress–strain curves were generated (Fig. 3b). The experimental results revealed pronounced anisotropic mechanical response in the insertion tissue specimens. Under low strain, when collagen fibers were still crimped and did not contribute to the strain energy, σ_x was larger due to the contribution from the bone side. However, when strains increased, collagen fibers straightened and aligned yielding significant contribution to the strain energy, therefore, longitudinal stress σ_z became larger.

To identify the material parameters for the GOH constitutive model (Eq. (1)–(3)), a computational model was created with material and structural grading described by Eq. (4)–(8). The dimension of the computational model was square (i.e., 5 mm x 5 mm) to better present the experiment setting (Fig. 3a). Because of the shape of the specimen, the condition of the mean fiber orientation tangential to the boundary (Eq. (8)), $\alpha_0(z)$ could not be used. Therefore $\alpha_0(z) = d\alpha_{max}$ was used where α_{max} was a given number — an angle achieved by the mean orientation of the fibers at the lower corner of the specimen, where insertion entered the bone [5]. For determinacy, it was taken as 90 degrees at the center of the model along the z -axis. The clamps were explicitly modeled in this geometry as shown by red contours in the inset of Fig. 3b, and displacement boundary conditions were applied to the clamp domains to simulate equibiaxial displacement-control mechanical testing. Because of the high inhomogeneity of stresses introduced in the areas between clamps [50], only the square region Ω in the center of the specimen was used to calculate average stress.

$$\sigma^{exp} = \int_{\Omega} \sigma(x, z) d\Omega \quad (9)$$

With the assumption of a linear variation for all material parameters across the z -axis, only six parameters were required for the GOH model to fully characterize tendon-to-bone insertion tissues. To further reduce the number of parameters, $c_t = 0.33$ MPa was adopted from Weiss et al. [51]. We also required that $k_{1t} \ll c_t$ to make sure that the nonlinear part of Eq. (2) did not contribute to the strain energy in the low strain region capturing ground matrix behavior.

By minimizing the average differences between the calculated and experimental stresses [52] and using the Matlab R2018b (MathWorks, Natick, Massachusetts, USA) optimization procedure *fminsearch* based on the Nelder–Mead algorithm, $f(\mathbf{S}^{pred}, \mathbf{S}^{exp}) = \sqrt{(\mathbf{S}^{pred} - \mathbf{S}^{exp})^2} / \sqrt{(\mathbf{S}^{exp})^2}$, where vectors \mathbf{S}^{pred} and \mathbf{S}^{exp} were defined as follows: $\mathbf{S}^{pred} = (\sigma_x^{pred}(\lambda_x), \sigma_z^{pred}(\lambda_x), \sigma_x^{pred}(\lambda_z), \sigma_z^{pred}(\lambda_z) \dots)$ and $\mathbf{S}^{exp} = (\sigma_x^{exp}(\lambda_x), \sigma_z^{exp}(\lambda_x), \sigma_x^{exp}(\lambda_z), \sigma_z^{exp}(\lambda_z) \dots)$, the parameters $k_{2t} = 0.04$, $c_b = 0.51$ MPa, $k_{1b} = 0.48$ MPa, and $k_{2b} = 0.15$ were identified. The experimental and predicted stress–strain curves are shown in Fig. 3b. One can observe that the anisotropic behavior was properly recovered: σ_x^{pred} was larger than σ_z^{pred} in the low strain region and then σ_z^{pred} became larger than σ_x^{pred} in the high strain region.

3.2. Stress distribution and fiber reorientation

With the obtained material parameters, graded material property, collagen fiber microstructure, and collagen fiber dispersion, a 2D geometry of the rotator-cuff joint model was then implemented (Fig. 2). To observe the stress distribution and fiber reorientations at the insertion region, the longitudinal displacement boundary conditions $u_z = 3.5$ cm were applied to the top end of the tendon, while the bottom edge of the bone was held fixed in the z -direction, but allowed to move along the x -direction, resulting in 50% total elongation of the structure. Based on the quantitative study by Burr et al. 1996, it was similar to a walking condition [53]. Quasi-static deformation of the structure was considered. To see the effect of graded collagen fiber microstructure, the model was compared to the case when the insertion region was not graded and had constant material properties, taking averaged values between tendon and bone tissues:

$$c_i = \frac{c_t + c_b}{2}, \quad k_{1i} = \frac{k_{1t} + k_{1b}}{2}, \quad k_{2i} = \frac{k_{2t} + k_{2b}}{2},$$

$$\kappa_i = \frac{\kappa_t + \kappa_b}{2} = 1/6, \quad (i = 1, 2).$$

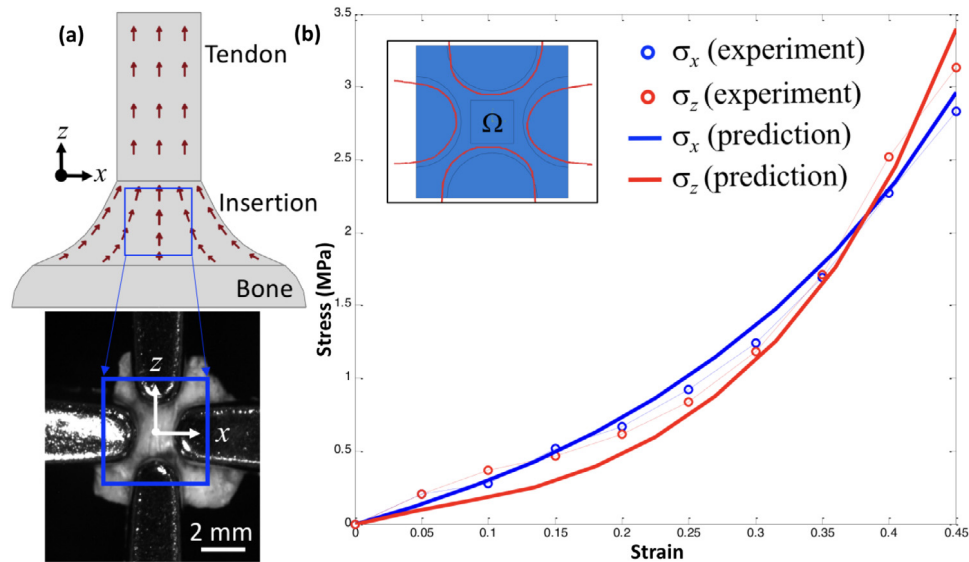


Fig. 3. (a) Biaxial mechanical testing setting for insertion tissues. (b) Stress–strain curves for insertion tissues, where nonlinear anisotropic mechanical properties were experimentally quantified (mean only and SEM were not shown; $n = 6$) and computationally fitted.

Fig. 4 shows the results of the computational simulation for the two cases: models with graded and non-graded material properties within the insertion region at different instances of quasi-normalized time $t = 0.3$, $t = 0.7$, and $t = 1$, where $t = 1$ indicating reaching 50% elongation. Fig. 4a and b revealed the von Mises stress distribution within the structures for the graded and non-graded cases, respectively. We chose von Mises stress as one of possible scalar measures of the stress state often used to predict onset of plasticity of damage, importantly this quantity neglected pressure in incompressible material. One could observe that models with graded material properties significantly reduced maximum von Mises stress and that the stress distribution was smoother in the insertion region. The maximum von Mises stress achieved at time $t = 1$ was 41.8 MPa in the graded material properties (Fig. 4a), and 46.4 MPa in the model with non-graded material properties (Fig. 4b), with 10% difference between the peak stresses. The stress results from the simulations suggested that the models with graded material properties could potentially reduce the chances of injury. It is important to keep this in mind when designing surgical interventions or tissue engineered implants. Fig. 4c and d showed the magnitude the angle differences between the final fiber orientation and the initial fiber orientation, $|\mathbf{a}(t = 1) - \mathbf{a}_0|$ for models with graded and non-graded material properties. Please note that to better demonstrate the changes in the fiber orientation for these 2 models, different scales were used. It showed that the mean fiber orientation for the model with graded material properties had caused zero fiber readjustments at the insertion boundary during deformations ($|\Delta \mathbf{a}| = 0$), but there was some fiber reorientation inside the insertion and tendon ($|\Delta \mathbf{a}| = 0.05$) (Fig. 4c). In the models with non-graded material properties, fibers were not tangential to the boundary initially and most reorientation occurred near the boundary ($|\Delta \mathbf{a}| = 0.16$) (Fig. 4d). The presence of such significant readjustments in fiber orientation also suggested the importance of using a nonlinear model for tendon-to-bone insertion tissues, taking into account large deformations and fiber rotations. Such readjustments in mean fiber orientation may not be seen in linear models [20], where the graded fiber orientation was considered, though only with a linear approximation.

3.3. Parametric study

Having identified material properties, one may pose the problem of finding the shape of the insertion region which will minimize stress. The shape of the insertion region may be represented by cubic splines

and parameterized by N control points on the boundary as shown in Fig. 5a. Assuming X coordinates equally spaced, we would need to find N parameters providing the best stress distribution. Here we restricted only to the simplest case: when there was only one point with coordinates $(X, Z = 0.5)$, and conducted a parametric study. A customized python script was written which generated the whole model geometry according to the parameter value X , meshed the elements, and assigned material properties. The script also calculated the maximum Mises stresses $\sigma_{MM} = |\sigma_{Mises}(x, z)|_{\infty}$ within the structure to characterize the stress distribution. Fig. 5 showed stress distribution and fiber rotations $|\mathbf{a}(t = 1) - \mathbf{a}_0|$ for models with four different insertion geometries: $(X, Z = 0.0, 0.5)$, $(X, Z = 0.2, 0.5)$, $(X, Z = 0.4, 0.5)$, and $(X, Z = 0.6, 0.5)$. Both graded (Fig. 5b) and non-graded (Fig. 5c) material properties were incorporated. It is observed that the insertion shapes have significant effects on stress distribution and the fiber reorientation for all models with graded (Fig. 5d) and non-graded (Fig. 5e) material properties, suggesting possible geometry variations for the insertion region during *in-vivo* tissue remodeling. This result was in agreement with conclusions from Liu et al. [1] where only linear isotropic non-graded material properties were used in the insertion region.

4. Discussion

We have developed a nonlinear anisotropic structural-based model of tendon–bone insertion tissue with explicit continuous distribution of structural and mechanical properties. We successfully adopted the Gasser–Ogden–Holzapfel (GOH) constitutive model [24,28–30] which was initially developed for arterial layers. Our study showed that modeling the tendon–bone insertion with the GOH model was particularly suitable, where spatial grading of structural parameters such as mean fiber orientation, fiber dispersion, and material parameters could be adopted.

Material parameters from the GOH models were obtained by minimizing the average differences between simulated and biaxial experimental stresses, imposing more realistic strains on the tissue as compared to uniaxial testing. The results of experiments and simulations recovered the characteristics of the anisotropic mechanical responses of the specimen: tissues exhibited larger stresses along the preferred fiber direction in the higher strain region (Fig. 3). This was due to collagen fiber recruiting that resulted from the spatial inhomogeneity of the material properties within the specimen. We have shown that graded structural and material properties reduced peak stresses

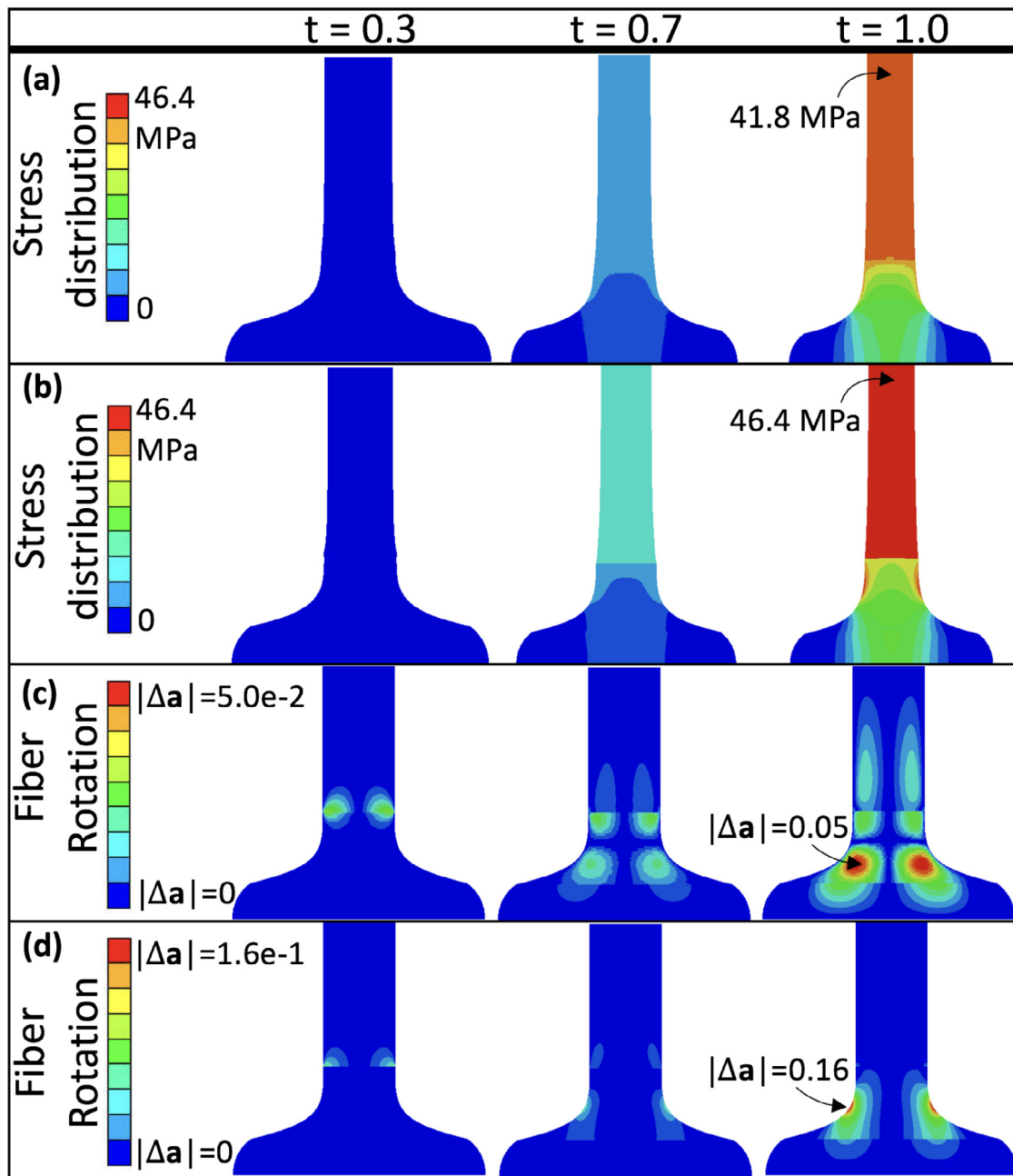


Fig. 4. Stress distributions for models with (a) graded and (b) non-graded materials properties at different instances in time. Fiber rotation within tendon, bone, and insertion regions for models with (c) graded and (d) non-graded materials properties at different instances in time.

and resulted in smoother stress distribution in the insertion region (Fig. 4), suggesting a potential for reduced chances of rupture. This has to be kept in mind when surgical interventions are planned. The results of the parametric study demonstrated that the optimal insertion shape depended on the graded material properties, where stresses are reduced when the angle between the tendon edge and bone edge at the interface was small. That is, models with $(X, Z = 0.0, 0.5)$ and $(X, Z = 0.2, 0.5)$ exhibited lower stress distributions and less fiber reorientations (Fig. 5).

In the current study, we used the maximum Mises stress as the criterion for the quality of the insertion region to dissipate stresses. To avoid stress concentrations, criteria needed to be established such that stress singularity occurs under large deformations. However, the damage criteria might depend greatly on the microstructure. For example, with the same stresses, the tissue was more likely to break at the tendon side than at the bone side. It is important to understand the damage and rupture mechanisms to prevent failures after surgeries.

Some computational issues arose during the modeling and optimal shape predictions. For example, mesh sensitivity at larger values of the shape parameter X and larger deformation (such values of parameter X and deformations are not considered in the present study) was related to stress concentrations. We may still have stress singularities even in the graded system because material properties within the elements were taken as constants at the integration points of each element. For better shape predictions, one would need a much smoother variation in material properties. This may be achieved by providing different material properties at different integration points within the finite elements using the User Defined Material (UMAT) procedure, by using a generalized continuum [54,55], or by incorporating material gradations into a non-local integration scheme, as developed by Fish and Kuznetsov [56,57] where a UEL procedure (*i.e.*, user subroutine to define an element) was used. Furthermore, mesh-size affect was not conducted in the current work and it is our study limitation.

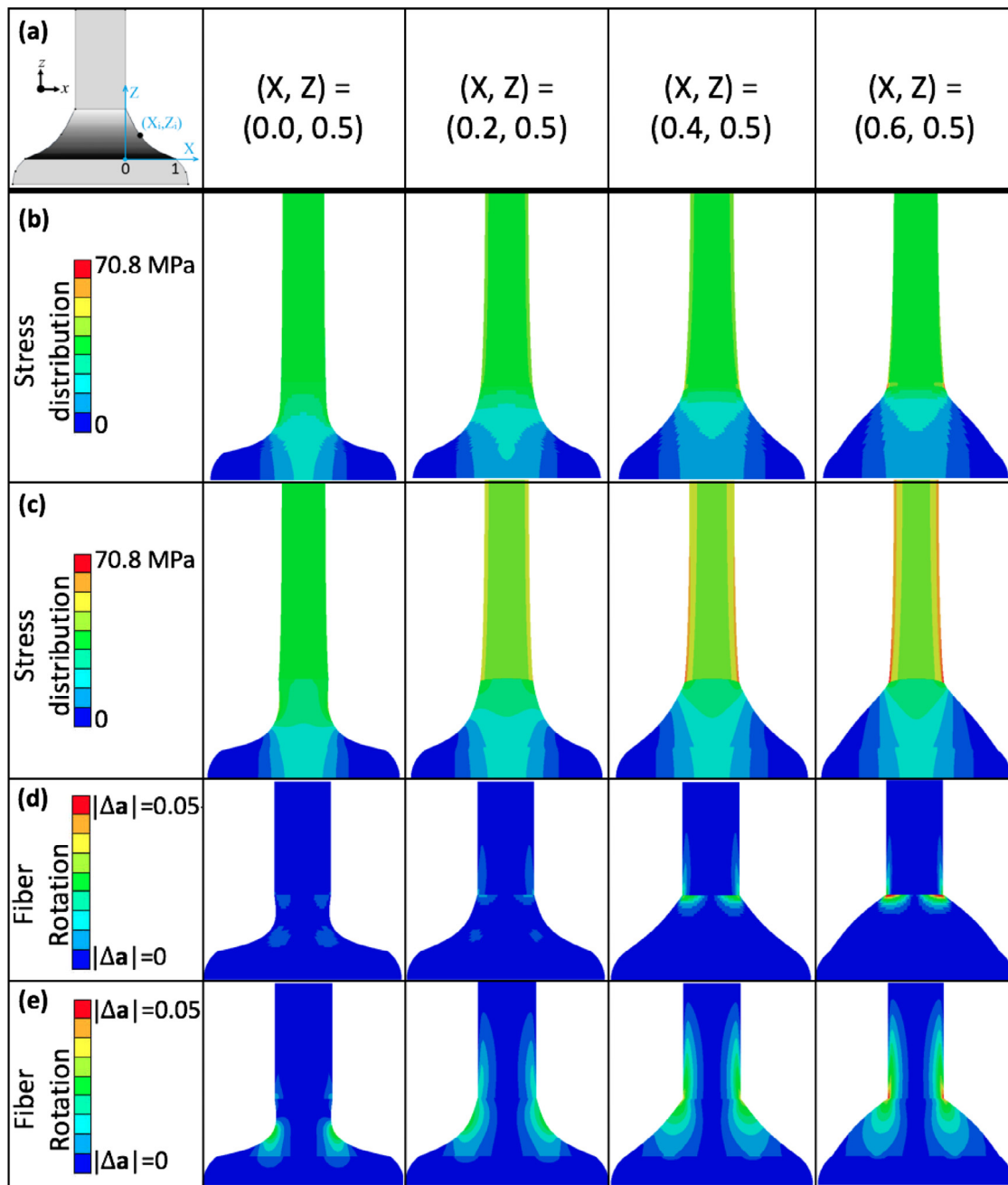


Fig. 5. (a) Shape optimization in the insertion region. Stress distributions for models with (b) graded and (c) non-graded materials properties. Changes in preferred material orientations for models with (d) graded and (e) non-graded materials properties.

In this work, we have chosen material and structural parameters that change linearly in space. However, actual distributions may not be linear or monotonic [2]. Therefore, we did not intend to obtain the elastic modulus of the bone to match with the actual one. Instead, we proposed a computational routine to characterize insertion tissues based on our assumptions of distributed material and structural properties. Moreover, we did not use the homogenization model proposed in Genin et al. and Liu et al. [2,23], as their models were developed with a linear approximation. Instead of adapting a nonlinear homogenization technique developed by Fish [53,54], Yvonnet, and their colleagues [58–61], we have developed models relating mineralization level and collagen fiber dispersion, as observed in experiments [5]. Nevertheless, more work needs to be done to determine actual material and structural variations within the insertion domain, such as using nonlinear imaging data for microstructures [62–64]. A 2D model was

developed in the current study. However, a 3D model is needed to properly reflect the complex states of stress and strain due to differences in the thickness of the tendon, bone, and insertion tissues [20], as well as the effect of surrounding tissues. In addition, viscoelasticity should be taken into account since it is a very important phenomena both in soft and hard biological tissues [17,65–67]. For that, we have developed rate-dependent viscoelastic models to describe tendon–bone insertion tissues [25].

5. Conclusions

Tendon-to-bone insertions may be considered as continuous functionally-graded connective tissue whose anisotropic biomechanical functions depend intimately on the regional biochemical composition and microstructure [2,5]. A structure-based model taking into account

continuous variations in material properties, fiber orientation, and fiber dispersion was developed. The GOH hyperelastic model was adopted and explicit grading of structural and material properties were implemented via a customized python script to introduce structural grading along preferred fiber orientation. Using this model, we were able to recover the unique anisotropic nonlinear mechanical responses of the tendon-to-bone insertion tissues as observed in experiments. We show that the continuous grading of structural and material properties resulted in a smoother stress distribution with smaller peak stresses than in the model with piecewise homogeneous material properties. The latter was often used when modeling tendon-to-bone insertion tissues by other research groups. We demonstrated the dependence of peak stresses on the gross shape of the insertion, which is important to take into account when age or occupation-related tendon-to-bone remodeling occurs. It helps us to understand how tendon-to-bone insertions function to dissipate stress generated at the interface of dissimilar materials. The study will be useful for controlling healing of the damaged insertion by utilizing proper mechanical and biological cues to regenerate original heterogeneous tissue structures. Further, this research will also help to develop biomimetic procedures to connect dissimilar materials in general. For example, where soft actuators of compliant mechanisms need to be connected to hard skeletal structures in robotics.

Declaration of competing interest

The authors declare that they have no known competing financial interests or personal relationships that could have appeared to influence the work reported in this paper.

Acknowledgments

The authors gratefully acknowledge Ms. Sandhya Chandrasekaran for her assistance with imaging histological samples and performing biaxial mechanical testing on tendon-bone insertion tissues. This work was supported by NSF CMMI-1400018. K. Peters was supported by the National Science Foundation while working at the foundation. Any opinion, finding, conclusions, or recommendations expressed in this material are those of the authors and do not necessarily reflect the views of the National Science Foundation.

References

- [1] Y. Liu, V. Birman, C. Chen, S. Thomopoulos, G.M. Genin, Mechanisms of bimaterial attachment at the interface of tendon to bone, *Trans. ASME, J. Eng. Mater. Technol.* 133 (1) (2011).
- [2] G.M. Genin, A. Kent, V. Birman, B. Wopenka, J.D. Pasteris, P.J. Marquez, S. Thomopoulos, Functional grading of mineral and collagen in the attachment of tendon to bone, *Biophys. J.* 97 (4) (2009) 976–985.
- [3] M. Benjamin, T. Kumai, S. Milz, B.M. Boszczyk, A.A. Boszczyk, J.R. Ralphs, The skeletal attachment of tendons - tendon 'entheses', *Comp. Biochem. Physiol. A* 133 (4) (2002) 931–945.
- [4] S. Thomopoulos, G.R. Williams, J.A. Gimbel, M. Favata, L.J. Soslowsky, Variation of biomechanical, structural, and compositional properties along the tendon to bone insertion site, *J. Orthop. Res.* 21 (3) (2003) 413–419.
- [5] S. Chandrasekaran, M. Pankow, K. Peters, H.S. Huang, Composition and structure of porcine digital flexor tendon-bone insertion tissues, *J. Biomed. Mater. Res. Part A* 105 (11) (2017) 3050–3058.
- [6] J. Apostolakos, T.J.S. Durant, C.R. Dwyer, R.P. Russel, J.H. Weinreb, F. Alaaee, K. Beitzel, M.B. McCarthy, M.P. Cote, A.D. Mazzocca, The enthesis: A review of the tendon-to-bone insertion, *Muscles Ligaments Tendons J.* 4 (3) (2014) 333–342.
- [7] H. Khayyeri, P. Blomgran, M. Hammerman, M.J. Turunen, A. Lowgren, M. Guizar-Sicairos, P. Aspenberg, H. Isaksson, Achilles tendon compositional and structural properties are altered after unloading by botox, *Sci. Rep.* 7 (1) (2017) 13067.
- [8] M. Lavagnino, M.E. Wall, D. Little, A.J. Banes, F. Guilak, S.P. Arnoczky, Tendon mechanobiology: Current knowledge and future research opportunities, *J. Orthop. Res.* 33 (6) (2015) 813–822.
- [9] Y. Lanir, Constitutive equations for fibrous connective tissues, *J. Biomech.* 16 (1) (1983) 1–12.

- [10] Y. Lanir, A structural theory for the homogeneous biaxial stress-strain relationships in flat collagenous tissues, *J. Biomech.* 12 (6) (1979) 423–436.
- [11] Y. Lanir, A microstructure model for the rheology of mammalian tendon, *J. Biomech. Eng. Trans. ASME* 102 (4) (1980) 332–339.
- [12] K.L. Billiar, M.S. Sacks, Biaxial mechanical properties of the natural and glutaraldehyde treated aortic valve cusp—Part I: Experimental results, *J. Biomech. Eng.* 122 (1) (2000) 23–30.
- [13] S.P. Reese, J.A. Weiss, Tendons and ligaments: Current state and future directions, in: S. De, W. Hwang, E. Kuhl (Eds.), *Multiscale Modeling in Biomechanics and Mechanobiology*, Springer, London, 2014, pp. 159–206.
- [14] T.M. Keaveny, E.F. Morgan, O.C. Yeh, in: M. Kutz (Ed.), *Bone Mechanics, Standard Handbook of Biomedical Engineering & Design*, McGraw-Hill, New York, 2004, p. 24.
- [15] M.P.G. Bostrom, A. Boskey, J.K. Kauffman, T.A. Einhorn, in: J.A. Buckwalter, T.A. Einhorn, S.R. Simon (Eds.), *Form and Function of Bone*, American Academy of Orthopaedic Surgeons, Rosemont, IL, 2000, pp. 319–370.
- [16] Y.C. Fung, *Biorheology of soft tissues*, *Biorheology* 10 (1973) 139–155.
- [17] Y.C. Fung, *Biomechanics: Mechanical Properties of Living Tissues*, Springer Verlag, New York, 1993.
- [18] R.W. Ogden, *Non-Linear Elastic Deformations*, E. Horwood, 1984.
- [19] A.E. Jakus, A.L. Rutz, S.W. Jordan, A. Kannan, S.M. Mitchell, C. Yun, K.D. Koube, S.C. Yoo, H.E. Whiteley, C.P. Richter, R.D. Galiano, W.K. Hsu, S.R. Stock, E.L. Hsu, R.N. Shah, Hyperelastic bone: A highly versatile, growth factor-free, osteoregenerative, scalable, and surgically friendly biomaterial, *Sci. Transl. Med.* 8 (358) (2016).
- [20] S. Thomopoulos, J.P. Marquez, B. Weinberger, V. Birman, G.M. Genin, Collagen fiber orientation at the tendon to bone insertion and its influence on stress concentrations, *J. Biomech.* 39 (10) (2006) 1842–1851.
- [21] E.M. Spiesz, P. Roschger, P.K. Zysset, Influence of mineralization and microporosity on tissue elasticity: experimental and numerical investigation on mineralized turkey leg tendons, *Calcif. Tissue Int.* 90 (4) (2012) 319–329.
- [22] Q. Liu, H. He, Z.F. Li, Y.D. Liu, Y. Ren, W.Q. Lu, J. Lu, E.A. Stach, J. Xie, Rate-dependent, Li-ion insertion/deinsertion behavior of LiFePO₄ cathodes in commercial 18650 LiFePO₄ cells, *ACS Appl. Mater. Inter.* 6 (5) (2014) 3282–3289.
- [23] Y.X. Liu, S. Thomopoulos, C.Q. Chen, V. Birman, M.J. Buehler, G.M. Genin, Modelling the mechanics of partially mineralized collagen fibrils, fibres and tissue, *J. R. Soc. Interface* 11 (92) (2014).
- [24] T.C. Gasser, R.W. Ogden, G.A. Holzapfel, Hyperelastic modelling of arterial layers with distributed collagen fibre orientations, *J. R. Soc. Interface* 3 (6) (2006) 15–35.
- [25] S. Kuznetsov, M. Pankow, K. Peters, H.S. Huang, Strain state dependent anisotropic viscoelasticity of tendon-to-bone insertion, *Math. Biosci.* 308 (2019) 1–7.
- [26] A.J.M. Spencer, Constitutive theory for strongly anisotropic solids, in: *Continuum Theory of the Mechanics of Fibre-Reinforced Composites*, 1984, pp. 1–32.
- [27] Z.W. Chen, P. Joli, Z.Q. Feng, Anisotropic hyperelastic behavior of soft biological tissues, *Comput. Methods Biomech. Biomed. Eng.* 18 (13) (2015) 1436–1444.
- [28] G.A. Holzapfel, T.C. Gasser, A viscoelastic model for fiber-reinforced composites at finite strains: Continuum basis, computational aspects and applications, *Comput. Methods Appl. Mech. Engrg.* 190 (2001) 4379–4403.
- [29] G.A. Holzapfel, T.C. Gasser, R.W. Ogden, A new constitutive framework for arterial wall mechanics and a comparative study of material models, *J. Elasticity* 61 (1–3) (2000) 1–48.
- [30] G.A. Holzapfel, T.C. Gasser, R.W. Ogden, Comparison of a multi-layer structural model for arterial walls with a fun-g-type model, and issues of material stability, *J. Biomech. Eng.-Trans. ASME* 126 (2) (2004) 264–275.
- [31] B.H. Ng, S.M. Chou, B.H. Lim, A. Chong, Strain rate effect on the failure properties of tendons, *Proc. Inst. Mech. Eng. H* 218 (H3) (2004) 203–206.
- [32] T.A.L. Wren, S.A. Yerby, G.S. Beaupre, D.R. Carter, Mechanical properties of the human Achilles tendon, *Clin. Biomech.* 16 (3) (2001) 245–251.
- [33] N. Yamamoto, K. Hayashi, Mechanical properties of rabbit patellar tendon at high strain rate, *Biomed. Mater. Res. Eng.* 8 (2) (1998) 83–90.
- [34] B. Purinya, V. Kasyanov, J. Volkolakov, R. Latsis, G. Teter, Biomechanical and structural properties of the explanted bioprosthetic valve leaflets, *J. Biomech.* 27 (1) (1994) 1–11.
- [35] D. Lo, I. Vesely, Biaxial strain analysis of the porcine aortic valve, *Ann. Thorac. Surg.* 60 (2 Suppl) (1995) S374–378.
- [36] I. Vesely, R. Noseworthy, Micro mechanics of the Fibrosa and the Ventricularis in Aortic Valve Leaflets, *J. Biomech.* 25 (1) (1992) 101–113.
- [37] I. Vesely, A mechanism for the decrease in stiffness of bioprosthetic heart valve tissues after cross-linking, *ASAIO J.* 42 (6) (1996) 993–999.
- [38] J.D. Humphrey, R.K. Strumpf, F.C. Yin, Determination of a constitutive relation for passive myocardium: I. A new functional form, *J. Biomech. Eng.* 112 (3) (1990) 333–339.
- [39] J.D. Humphrey, *Cardiovascular Solid Mechanics: Cells, Tissues, and Organs*, Springer, New York, 2002.
- [40] J.D. Humphrey, Continuum biomechanics of soft biological tissues, *Proc. R. Soc. A* 459 (2029) (2003) 3–46.

- [41] H.-Y.S. Huang, B.N. Balhouse, S. Huang, Application of simple biomechanical and biochemical tests to heart valve leaflets: Implications for heart valve characterization and tissue engineering, *Proc. Inst. Mech. Eng. H* 226 (H11) (2012) 868–876.
- [42] H.-Y.S. Huang, S. Huang, C.P. Frazier, P. Prim, O. Harrysson, Directional mechanical property of porcine skin tissues, *J. Mech. Med. Biol.* 14 (5) (2014).
- [43] S. Huang, H.-Y.S. Huang, Biaxial stress relaxation of semilunar heart valve leaflets during simulated collagen catabolism: Effects of collagenase concentration and equibiaxial strain-state, *Proc. Inst. Mech. Eng. H* 229 (10) (2015) 721–731.
- [44] H.S. Huang, J. Lu, Biaxial mechanical properties of bovine jugular venous valve leaflet tissues, *Biomech. Model Mechanobiol.* (2017).
- [45] N. Kaul, H.S. Huang, Constitutive modeling of jugular vein-derived venous valve leaflet tissues, *J. Mech. Behav. Biomed. Mater.* 75 (2017) 50–57.
- [46] J. Lu, H.S. Huang, Biaxial mechanical behavior of bovine saphenous venous valve leaflets, *J. Mech. Behav. Biomed. Mater.* 77 (2018) 594–599.
- [47] S.E. Szczesny, J.M. Peloquin, D.H. Cortes, J.A. Kadlowec, L.J. Soslowsky, D.M. Elliott, Biaxial tensile testing and constitutive modeling of human supraspinatus tendon, *J. Biomech. Eng.* 134 (2) (2012) 021004.
- [48] N.T. Jacobs, D.H. Cortes, E.J. Vresilovic, D.M. Elliott, Biaxial tension of fibrous tissue: Using finite element methods to address experimental challenges arising from boundary conditions and anisotropy, *J. Biomech. Eng.-Trans. ASME* 135 (2) (2013).
- [49] B.B. Danley, H.-Y.S. Huang, Biomechanical and biochemical study of muscle-tendon-bone in porcine digital flexor tendon, *Proc. ASME International Mechanical Engineering Congress and Exposition Proceeding*.
- [50] W. Sun, M.S. Sacks, M.J. Scott, Effects of boundary conditions on the estimation of the planar biaxial mechanical properties of soft tissues, *J. Biomech. Eng.-Trans. ASME* 127 (4) (2005) 709–715.
- [51] J.A. Weiss, J.C. Gardiner, C. Bonifasi-Lista, Ligament material behavior is nonlinear, viscoelastic and rate-independent under shear loading, *J. Biomech.* 35 (7) (2002) 943–950.
- [52] J. Bergstrom, *Mechanics of solid polymers*, in: *Theory and Computational Modeling*, Elsevier, 2015.
- [53] D.B. Burr, C. Milgrom, D. Fyhrie, M. Forwood, M. Nyska, A. Finestone, S. Hoshaw, E. Saiag, A. Simkin, In vivo measurement of human tibial strains during vigorous activity, *Bone* 18 (5) (1996) 405–410.
- [54] M.G.D. Geers, V.G. Kouznetsova, W.A.M. Brekelmans, Multiscale first-order and second-order computational homogenization of microstructures towards continua, *Int. J. Multiscale Com.* 1 (4) (2003) 371–386.
- [55] A. Anthoine, Second-order homogenisation of functionally graded materials, *Int. J. Solids Struct.* 47 (11–12) (2010) 1477–1489.
- [56] J. Fish, V. Filonova, S. Kuznetsov, Micro-inertia effects in nonlinear heterogeneous media, *Internat. J. Numer. Methods Engrg.* 91 (13) (2012) 1406–1426.
- [57] J. Fish, S. Kuznetsov, Computational continua, *Internat. J. Numer. Methods Engrg.* 84 (7) (2010) 774–802.
- [58] J. Fish, R. Fan, Mathematical homogenization of nonperiodic heterogeneous media subjected to large deformation transient loading, *Internat. J. Numer. Methods Engrg.* 76 (7) (2008) 1044–1064.
- [59] S. Kuznetsov, J. Fish, Mathematical homogenization theory for electroactive continuum, *Internat. J. Numer. Methods Engrg.* 91 (11) (2012) 1199–1226.
- [60] J. Yvonnet, D. Gonzalez, Q.C. He, Numerically explicit potentials for the homogenization of nonlinear elastic heterogeneous materials, *Comput. Methods Appl. Mech. Engrg.* 198 (33–36) (2009) 2723–2737.
- [61] B.A. Le, J. Yvonnet, Q.C. He, Computational homogenization of nonlinear elastic materials using neural networks, *Internat. J. Numer. Methods Engrg.* 104 (12) (2015) 1061–1084.
- [62] A.A. Oberai, N.H. Gokhale, S. Goenezen, P.E. Barbone, T.J. Hall, A.M. Sommer, J.F. Jiang, Linear and nonlinear elasticity imaging of soft tissue in vivo: demonstration of feasibility, *Phys. Med. Biol.* 54 (5) (2009) 1191–1207.
- [63] S. Goenezen, P. Barbone, A.A. Oberai, Solution of the nonlinear elasticity imaging inverse problem: The incompressible case, *Comput. Methods Appl. Mech. Engrg.* 200 (13–16) (2011) 1406–1420.
- [64] S.W. Shore, P.E. Barbone, A.A. Oberai, E.F. Morgan, Transversely isotropic elasticity imaging of cancellous bone, *J. Biomech. Eng.-Trans. ASME* 133 (6) (2011).
- [65] K. Barbour, H.-Y.S. Huang, Strain effects on collagen proteolysis in heart valve tissues, *Mech. Time-Dep. Mater.* 23 (2) (2019).
- [66] E. Pena, B. Calvo, M.A. Martinez, M. Doblare, An anisotropic visco-hyperelastic model for ligaments at finite strains. formulation and computational aspects, *Int. J. Solids Struct.* 44 (3–4) (2007) 760–778.
- [67] R.S. Lakes, *Viscoelastic Solids*, CRC Press, New York, 1999.